Mathematical appendix: modeling mechanochemical coupling in cell polarity maintenance

Ondrej Maxian

March 19, 2024

1 Maintenance-phase as a steady state

1.1 CDK-1 (RNAi)

By treating embryos with *CDK-1* (RNAi), we can extend maintenance phase and determine whether the myosin and flow profiles we see in wild-type embryos are true steady states. Figs. **??** and **??** show the myosin intensity and pattern of flow over the last eight minutes of the extended maintenance phase. What is strange about this data is that the myosin intensities *never* look like the wild-type. There appears to be more than the expected amount of myosin on the posterior domain. An interesting observation also is that extending maintenance causes the boundary to move to the *right*.

2 Stability of myosin in maintenance phase

To understand the threshold for instability of Eq. (1) in the main text, we first define the cytoplasmic concentration via conservation of total protein

$$M_{\text{cyto}} = \frac{1}{hL}\left(M^{(\text{Tot})}L - \int_0^L M(x)\,dx\right), \tag{M1}$$

where L is the domain length, h is the cytoplasmic thickness, and $M^{(\text{Tot})}$ is the density of myosin on the cortex when all of it is bound. We then scale the equations by appropriate time ($1/k_M^{\text{off}}$), length (L), density ($M^{(\text{Tot})}$), and velocity ($\sigma_0/\sqrt{\eta\gamma}$) scales. Defining the dimensionless (hatted) variables

$$x = \hat{x}L \qquad t = \hat{t}/k_M^{\text{off}} \qquad M = \hat{M}M^{(\text{Tot})} \qquad v = \hat{v}\frac{\sigma_0}{\sqrt{\eta\gamma}}, \tag{M2}$$

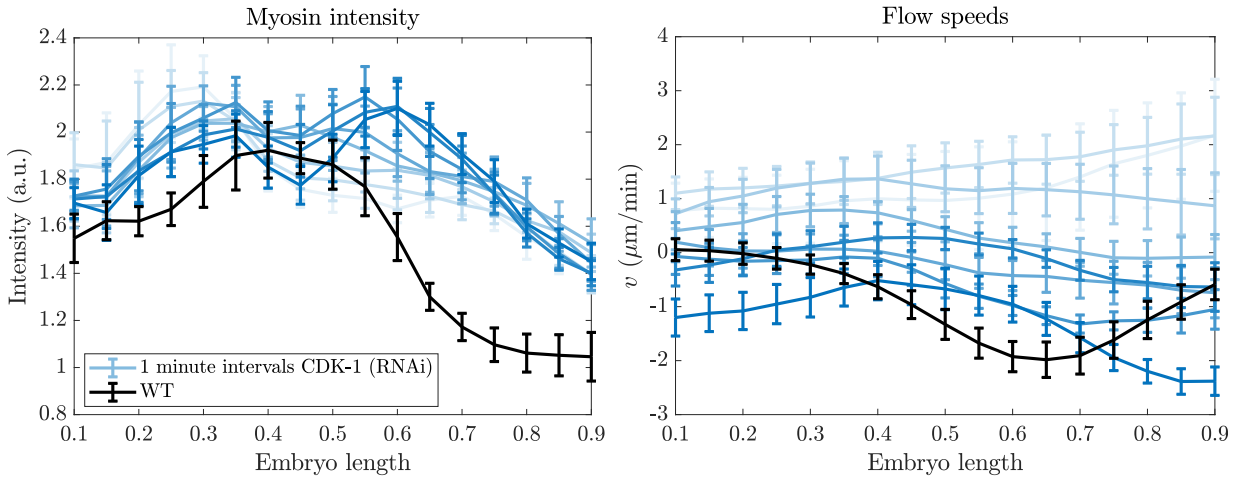

Figure M1: Comparing the end of maintenance phase in *CDK-1* (RNAi) mutants to wild-type embryos. Left panel: myosin intensity profile. Right panel: flow speeds. The blue colored lines show 1-minute intervals of maintenance phase in *CDK-1* (RNAi) embryos, with darker blue denoting later times. The black line shows the profile extracted from the last minute of maintenance phase in wild type embryos [10].

the resulting equations are

$$\partial_{\hat{t}}\hat{M} + \hat{\sigma}_0\partial_{\hat{x}}\left(\hat{v}\hat{M}\right) = \hat{D}_M\partial_{\hat{x}}^2\hat{M} + \hat{K}_M^{\text{on}}\left(1 - \int_0^1 \hat{M}(x)\,dx\right) - \hat{M} \tag{M3a}$$

$$\hat{v} = \hat{\ell}^2\partial_{\hat{x}}^2\hat{v} + \hat{\ell}\partial_{\hat{x}}\hat{\sigma}_a(\hat{M}) \tag{M3b}$$

and are controlled by the dimensionless parameters

$$\hat{\sigma}_0 = \left(\frac{\sigma_0/\sqrt{\eta\gamma}}{Lk_M^{\text{off}}}\right) \qquad \hat{D}_M = \frac{D_M}{k_M^{\text{off}}L^2} \qquad \hat{K}_M^{\text{on}} = \frac{k_M^{\text{on}}}{hk_M^{\text{off}}} \qquad \hat{\ell} = \frac{\sqrt{\eta/\gamma}}{L}. \tag{M4}$$

Recalling that $1/k_M^{\text{off}}$ is the residence time, these dimensionless parameters can be understood in the following way:

1. $\hat{\sigma}_0$ is the fraction of the domain over which a given myosin molecule is transported while it is bound to the membrane (the residence time $1/k_M^{\text{off}}$ $\times$ the advective velocity $\sigma_0/\sqrt{\eta\gamma}$).

2. $\hat{D}_M$ is the maximum fraction of the domain a molecule diffuses before it unbinds (in the extreme case when the gradient in the domain is $1/L$, the diffusive velocity is D_M/L).

3. $\hat{K}_M^{\text{on}}$ sets the uniform steady state of the model by $\hat{M}_0 = \hat{K}_M^{\text{on}}/\left(1 + \hat{K}_M^{\text{on}}\right)$.

4. $\hat{\ell}$ is the ratio of the hydrodynamic lengthscale (the lengthscale on which fluid flows can "grab" neighboring molecules) to the domain length.

Parameter	Description	Value	Units	Ref	Notes
L	Domain length	134.6	μm	[2]	radii 27×15 μm ellipse
D_M	Myosin diffusivity	0.05	$\mu\text{m}^2/\text{s}$	[3]	
$\hat{K}_M^{\text{on}}$	Myosin attachment rate	0.4			Fit to get 30% bound myosin
k_M^{off}	Myosin detachment rate	0.12	1/s	[3]	
η	Cytoskeletal fluid viscosity	0.1	Pa·s		$100 \times$ water
γ	Myosin drag coefficient	5×10^{-4}	$\text{Pa·s}/\mu\text{m}^2$		$\ell = \sqrt{\eta/\gamma} = 14\,\mu$m [7]
σ_0	Stress coefficient and form	0.0071	Pa		Fit in Sec. 2.1.1
$\hat{\sigma}_a(\hat{M})$	Stress function of myosin	$\hat{M}$			Fit in Sec. 2.1.1

Table 1: Parameter values for myosin model. Parameters listed with a citation are lifted directly from the corresponding study. See Section 2.1 for a discussion of the fitting procedure for the other parameters.

Prior to performing linear stability analysis, we need to first determine the function σ_a and the other parameters.

2.1 Parameter estimation

Table 1 lists the parameters for the myosin model. According to [2], the *C. elegans* embryo has a roughly ellipsoidal shape, with half-axis lengths $27 \times 15 \times 15$ μm. The in-membrane diffusivity of myosin, as well as the detachment rate, have both been measured in [3]. For the attachment rate, it was estimated in [3, Fig. S3m] that roughly 30% of myosin is bound to the cortex in wild-type embryos. Recalling that the uniform steady state is $\hat{M}_0 = \hat{K}_M^{\text{on}} / \left(1 + \hat{K}_M^{\text{on}}\right)$, this gives $\hat{K}_M^{\text{on}} = 0.43$. The total amount of myosin scales out of the equations.

For the fluid parameters, we assume that the viscosity of the cytoskeletal fluid on the cortex is 100 times water, which gives 0.1 Pa·s. The "hydrodynamic length scale" of $\ell = \sqrt{\eta/\gamma} = 14$ μm, measured in [7, 9], then gives the myosin drag coefficient γ. But more important than either of these is the stress as a function of myosin concentration. We fit this from the wild-type data of [10] in the next section.

2.1.1 Inferring flow profile from experiments

Because we can measure the cortical velocity and myosin intensity, we can actually infer the function $\sigma_a(M)$ in dimensional units from the experimental data [10]. We in particular isolate the myosin intensity and flow speed during late maintenance phase in wild type embroys [10, Fig. 1B(bottom)],

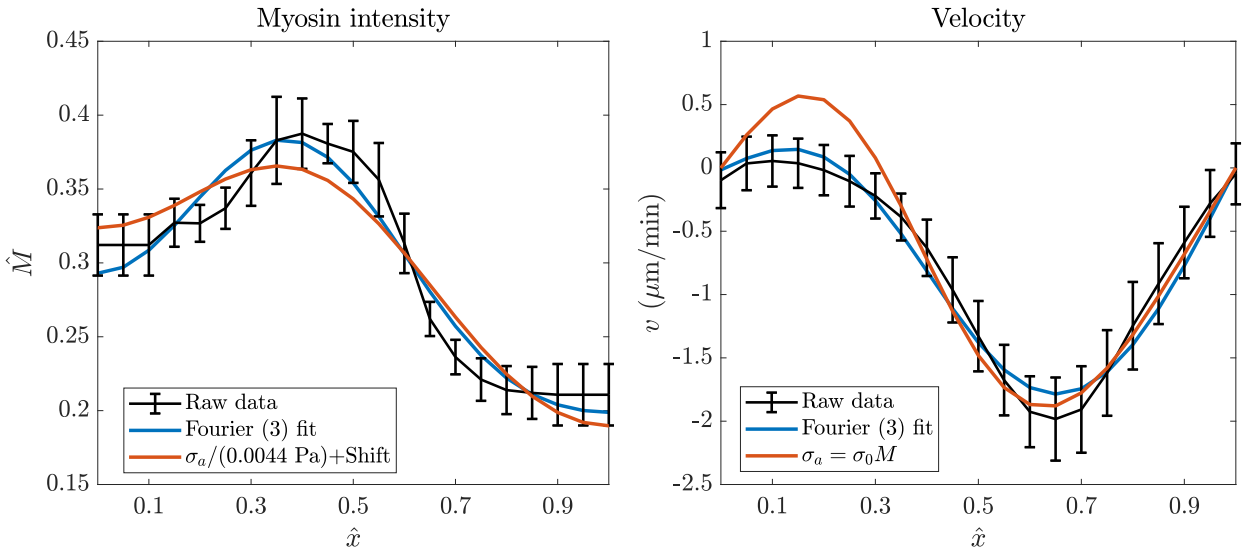

Figure M2: Extracting the active stress from the velocity profile. Left: the experimental data for myosin intensity (black with the outer 10% of the embryo on each side adjusted to be constant) and Fourier fit (blue), compared to the fitted stress (red). Right: velocity in μm/min (black) and Fourier fit (blue), compared to the velocity obtained when $\sigma_a = \sigma_0 M$.

plotting the results in black in Fig. M2. For the myosin intensity, we normalize so that the mean amount of bound myosin is 0.3 [3, Fig. S3], and adjust for the sensitivity of our measurements near the embryo edges by setting the myosin intensity at the outer 10% of the embryo to be constant and equal to that measured at the 10% boundary. We then periodically extend this data so that we fill the whole circumference (2 embryo lengths), and fit with a 3-term (4 terms including the constant) Fourier series.

To extract the stress profile from the smoothed velocity and myosin intensity, we consider a hybrid dimensional form of the velocity equation ((1b) in main text)

$$\gamma v - \frac{\eta}{L^2}\partial_{\hat{x}}^2 v = \frac{1}{L}\partial_{\hat{x}}\sigma_a(M).$$

Let the Fourier series representation for $v(\hat{x}) = \sum_k \tilde{v}(k)\exp(2\pi i k\hat{x})$, and likewise for $\hat{\sigma}_a$. Then, in Fourier space, the solution for σ_a is given by

$$\sigma_a(k) = \frac{\gamma + \eta/L^2\,(2\pi k)^2}{2\pi i k/L}\tilde{v}(k). \tag{M5}$$

The $k = 0$ mode is undefined because σ_a only appears differentiated; thus stress is only available up to an arbitrary constant.

We insert the parameters from Table 1 into (M5), then rescale the resulting stress by $\sigma_0 = 4.4 \times 10^{-3}$ Pa plus an arbitrary constant, so that it aligns with the myosin intensity we determined

experimentally. The left panel of Fig. M2 demonstrates that we can set

$$\hat{\sigma}_a = \hat{M} \tag{M6}$$

as a good approximation to the (dimensionless) stress. Using $\sigma_0 = 4.4\times10^{-3}$ Pa and the parameters in Table 1, the dimensionless parameter $\hat{\sigma}_0$ defined in (M4) is therefore equal to

$$\hat{\sigma}_0 = \left(\frac{\sigma_0/\sqrt{\eta\gamma}}{Lk_M^{\text{off}}}\right) \approx 0.04, \tag{M7}$$

which will control the stability analysis in the next section.

Prior to doing this, we make the observation that inserting the wild-type stress $\sigma_a = \sigma_0 M$ into the velocity equation gives the velocity profile shown in red in the right panel of Fig. M2. In the posterior, we obtain a velocity profile which perfectly matches the data. In the anterior, on the other hand, there is a clear mismatch where the model predicts more contractility (flows into the myosin peak) than the data show. This demonstrates that there are additional agents inhibiting contractility in the anterior. We will address the source of this ambiguity in Section 4.

2.2 Linear stability analysis

Now that all the parameters are known, we can perform linear stability analysis to see if the system could spontaneously polarize. The uniform steady state is $\hat{M}_0 = \hat{K}_M^{\text{on}}/\left(1+\hat{K}_M^{\text{on}}\right)$. We consider a perturbation around that state $\hat{M} = \hat{M}_0 + \delta\hat{M}$, where $\delta\hat{M} = \delta\hat{M}_0 e^{\lambda(k)\hat{t}+2\pi ik\hat{x}}$. Plugging this into (M3b), we get the velocity [1, Eq. (11)]

$$\hat{v} = \frac{2\pi ik\hat{\ell}\hat{\sigma}_a'(\hat{M}_0)}{1+\left(2\pi k\hat{\ell}\right)^2}\hat{\delta}M. \tag{M8}$$

Substituting this velocity into (M3a), and considering only the first order terms, we get the following equation for the eigenvalues

$$\lambda(k) = \frac{4\pi^2k^2\hat{\ell}\hat{M}_0\hat{\sigma}_0\hat{\sigma}_a'(\hat{M}_0)}{1+4\pi^2k^2\hat{\ell}^2} - \hat{D}_M 4\pi^2k^2 - 1 \tag{M9}$$

Using the parameters in Table 1, we have the following values for the dimensionless groups

$$\hat{D}_M = 2.3\times10^{-5} \qquad \hat{M}_0 \approx 0.3 \qquad \hat{\sigma}_a' = 1 \qquad \hat{\ell} \approx 0.07. \tag{M10}$$

Substituting these parameters into the dispersion relation (M11) gives the eigenvalues $\lambda(k)$ shown in Fig. M3 as a function of wavelength k and dimensionless flow speed $\hat{\sigma}_0$. We observe strong flow

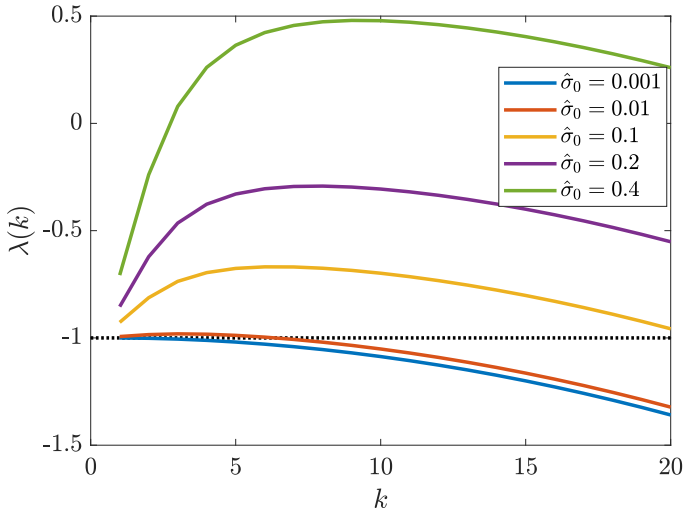

Figure M3: Stability analysis for myosin model (M3). We consider perturbations of size proportional to $e^{\lambda(k)\hat{t}+2\pi ik\hat{x}}$, then solve the linearized form of (M3) to obtain $\lambda(k)$ in (M11). Positive (negatve) eigenvalues indicate instability (stability) of the steady state.

coupling required for instability; with $\hat{\sigma}_0 = 0.2$ (flow transports myosins around 20% of the cell before they come off), the dynamics remain stable. Our estimate $\hat{\sigma}_0 \approx 0.04$ clearly demonstrates that myosin cannot self-polarize in the zygote.

Importantly, the large value of $\hat{\sigma}_0$ needed for instability is a consequence of the -1 in the dispersion relation (M11), which comes from the unbinding kinetics. Thus, unbinding makes it *harder* to destabilize the uniform steady state. Indeed, without the -1, the instability occurs at $\hat{\sigma}_0 \approx 10^{-3}$, which is pretty weak coupling to the flow (and weaker coupling than we observe experimentally). When we account for unbinding, diffusion becomes so small as to be irrelevant, as for the $k = 1$ mode the coefficient in (M11) is $\hat{D}_M 4\pi^2 \approx 10^{-3}$. Thus, the real balance here (to generate the instability) is not between advection and diffusion, but between advection and *unbinding*.

When we neglect diffusion in (M11), the largest eigenvalues occur when k is largest, so we an effectively take a limit as $k \to \infty$ to obtain

$$\lambda(k) = \frac{\hat{M}_0 \hat{\sigma}_0 \hat{\sigma}_a'}{\hat{\ell}^2} - 1 = \frac{\hat{M}_0 \left(\sigma_0/\sqrt{\eta\gamma}\right)}{\ell k_M^{\text{off}}} - 1 \tag{M11}$$

Recognizing $\sigma_0/\sqrt{\eta\gamma}$ as the velocity scale v, the condition $\lambda(k) > 0$ becomes equivalent to $v/k_M^{\text{off}} > \ell/\hat{M}_0$. The main text discusses the most extreme case when $\hat{M}_0 = 1$ (all myosin bound to the membrane).

3 Maintenance phase biochemistry model

We now turn to parameter fitting on the biochemistry model (2) in the main text. To fit missing parameters, we repeat the non-dimensionalization procedure we used for the myosin equation in Section 2 and in [5] for the PAR-3 equations. We scale lengths by L, time by k_A^{dp} (the typical time a molecule of PAR-3 spends on the membrane), and concentrations by the maximum when all protein is bound ($X^{(\mathrm{Tot})}$ for protein X). The resulting dimensionless equations are

$$\partial_{\hat{t}}\hat{A}_1 = \hat{D}_A\partial_{\hat{x}}^2 A_1 + \hat{K}_A^{\mathrm{on}}\left(1+\hat{K}_A^{\mathrm{f}}\hat{F}_A(\hat{A})\right)\left(1-\int_0^1 \hat{A}(x)\,d\hat{x}\right) - \hat{K}_A^{\mathrm{off}}\hat{A}_1 \tag{M12a}$$

$$+ 2\hat{A}_2 - 2\hat{K}_A^{\mathrm{p}}(\hat{P})\hat{A}_1{}^2 + \sum_{n=3}^{N}\left(\hat{A}_n - \hat{K}_A^{\mathrm{p}}(\hat{P})\hat{A}_1\hat{A}_{n-1}\right) \tag{M12b}$$

$$\partial_{\hat{t}}\hat{A}_n = \hat{K}_A^{\mathrm{p}}(\hat{P})\hat{A}_1(\hat{A}_{n-1}-\hat{A}_n) - (\hat{A}_n - \hat{A}_{n+1}) \qquad N > n \geq 2 \tag{M12c}$$

$$\partial_t\hat{A}_N = \hat{K}_A^{\mathrm{p}}(\hat{P})\hat{A}_1\hat{A}_{N-1} - \hat{A}_N, \tag{M12d}$$

for PAR-3, which are exactly those we used in [5], except that now the net polymerization rate $\hat{K}_{\mathrm{AP}}^{\mathrm{p}}$ is a function of P. To account for the inhibition of PAR-3 cluster growth by PAR-1 (P), we increase the effective depolymerization rate by setting

$$\hat{K}_{\mathrm{AP}}^{\mathrm{p}}(\hat{P}) = \frac{k_A^{\mathrm{p}}A^{(\mathrm{Tot})}}{k_A^{\mathrm{dp}}\left(1+\hat{R}_{\mathrm{PA}}\hat{P}\right)} := \frac{\hat{K}_A^{\mathrm{p}}}{1+\hat{R}_{\mathrm{PA}}\hat{P}} \tag{M12e}$$

where $\hat{R}_{\mathrm{PA}} = r_{\mathrm{PA}}P^{(\mathrm{Tot})}/k_A^{\mathrm{dp}}$ describes the rate at which pPARs inhibit cluster accumulation relative to the normal rate of depolymerization k_A^{dp}. When $\hat{R}_{\mathrm{PA}} = 0$, we recover the dimensionless grouping $\hat{K}_A^{\mathrm{p}}$ used in [5]. Thus, all of the dimensionless parameters in the PAR-3 equations,

$$\hat{D}_A = \frac{D_A}{L^2k_A^{\mathrm{dp}}}, \quad \hat{K}_A^{\mathrm{on}} = \frac{k_A^{\mathrm{on}}}{k_A^{\mathrm{dp}}h}, \quad \hat{K}_A^{\mathrm{f}} = \frac{k_A^{+}A^{(\mathrm{Tot})}}{k_A^{\mathrm{on}}}, \quad \hat{K}_A^{\mathrm{off}} = \frac{k^{\mathrm{off}}}{k_A^{\mathrm{dp}}} \qquad \hat{K}_A^{\mathrm{p}} = \frac{k_A^{\mathrm{p}}A^{(\mathrm{Tot})}}{k_A^{\mathrm{dp}}},$$

with the exception of $\hat{R}_{\mathrm{PA}}$, are known from [5]. We do not repeat their values here.

The dimensionless forms of the equations for CDC-42, PAR-6/PKC-3, and pPARs are

$$\partial_{\hat{t}}\hat{C} = \hat{D}_C\partial_{\hat{x}}^2\hat{C} + \hat{K}_C^{\mathrm{on}}\left(1-\int_0^1\hat{C}(\hat{x})\,d\hat{x}\right) - \hat{K}_C^{\mathrm{off}}\left(1+\hat{R}_{\mathrm{PC}}\hat{P}\right)\hat{C} \tag{M12f}$$

$$\partial_{\hat{t}}\hat{K} = \hat{D}_K\partial_{\hat{x}}^2\hat{K} + \hat{R}_{\mathrm{ACK}}\hat{C}\delta_{\hat{A}>\hat{A}_0}\left(1-\int_0^1\hat{K}(\hat{x})\,d\hat{x}\right) - \hat{K}_K^{\mathrm{off}}\hat{K} \tag{M12g}$$

$$\partial_{\hat{t}}\hat{P} = \hat{D}_P\partial_{\hat{x}}^2\hat{P} + \hat{K}_P^{\mathrm{on}}\left(1-\int_0^1\hat{P}(\hat{x})\,d\hat{x}\right) - \hat{K}_P^{\mathrm{off}}\left(1+\hat{R}_{\mathrm{KP}}\hat{K}\right)\hat{P}. \tag{M12h}$$

Parameter	Description	Value	Units	Ref	Notes
D_P	pPAR diffusivity	0.15	$\mu\text{m}^2/\text{s}$	[2]	
D_K	PAR-6 diffusivity	0.1	$\mu\text{m}^2/\text{s}$	[8]	
D_C	CDC-42 diffusivity	0.1	$\mu\text{m}^2/\text{s}$		Same as PAR-6
k_P^{off}	pPAR detachment rate	7.3×10^{-3}	1/s	[2]	
k_K^{off}	PAR-6 detachment rate	0.01	1/s	[8]	
k_C^{off}	CDC-42 detachment rate	0.01	1/s		Same as PAR-6
$\hat{K}_P^{\text{on}}$	PAR-2 attachment rate	0.09			$P \approx 1$ in enrichment zone
$\hat{R}_{\text{KP}}$	K inhibiting P	50			Strong inhibition
$\hat{R}_{\text{PC}}$	P inhibiting C	(M15)		[10]	CDC/CHIN-1 relationship (Fig. A5)
$\hat{K}_C^{\text{on}}$	CDC-42 attachment rate	0.07			20% bound with inhibition
$\hat{A}_0$	PAR-3 threshold for PAR-6	0.06		[10]	10% anterior level
$\hat{R}_{\text{ACK}}$	A and C creating K	0.1			20% bound K
$\hat{R}_{\text{PA}}$	P inhibiting A	2			α on posterior in wild-type

Table 2: Additional parameter values for the biochemistry model.

These equations reveal the following dimensionless groups

$$\hat{R}_{\text{PC}} = \frac{r_{\text{PC}} P^{(\text{Tot})}}{k_C^{\text{off}}}, \quad \hat{R}_{\text{ACK}} = \frac{r_{\text{ACK}} C^{(\text{Tot})}}{k_A^{\text{dp}} h}, \quad \hat{R}_{\text{KP}} = \frac{r_{\text{KP}} K^{(\text{Tot})}}{k_P^{\text{off}}} \tag{M13a}$$

$$\hat{K}_P^{\text{on}} = \frac{k_P^{\text{on}}}{k_A^{\text{dp}} h}, \quad \hat{K}_C^{\text{on}} = \frac{k_C^{\text{on}}}{k_A^{\text{dp}} h}, \quad \hat{A}_0 = \frac{A_0}{A^{(\text{Tot})}} \tag{M13b}$$

$$\hat{D}_P = \frac{D_P}{L^2 k_A^{\text{dp}}}, \quad \hat{D}_C = \frac{D_C}{L^2 k_A^{\text{dp}}}, \quad \hat{D}_K = \frac{D_K}{L^2 k_A^{\text{dp}}}, \quad \hat{K}_P^{\text{off}} = \frac{k_P^{\text{off}}}{k_A^{\text{dp}}}, \quad \hat{K}_K^{\text{off}} = \frac{k_K^{\text{off}}}{k_A^{\text{dp}}}, \quad \hat{K}_C^{\text{off}} = \frac{k_C^{\text{off}}}{k_A^{\text{dp}}} \tag{M13c}$$

Among these, the parameters in (M13c) are all known from literature, and have been reported in the top half of Table 2. This leaves the six parameters in (M13a) and (M13b), which we determine sequentially from the following set of experimental observations:

1. In embryos without myosin flows, roughly 25–30% of the available PAR-2 is bound at steady state [3, Fig. S3]. Because the PAR-2 domain is only 25–30% of the embryo, the concentration of P in its enrichment zone must be near 1. We find that $\hat{K}_P^{\text{on}} = 0.09$ reproduces this result (in dimensional units $k_P^{\text{on}} = 0.13$ μm/s [3]).

2. In embryos without myosin flows, the level of PAR-2 at the anterior is no more than 5% of the posterior level [3, Fig. 2c]. This sets $\hat{R}_{\text{KP}} \gg 1$. We use $\hat{R}_{\text{KP}} = 50$ for strong inhibition.

3. The parameter $\hat{R}_{\text{PC}}$ is available from the data in [10]. To obtain it, we solve (M12f) at steady

state to obtain

$$\hat{C} = \frac{1}{1 + \frac{h k_c^{\text{off}}}{k_C^{\text{on}}} + \frac{\hat{R}_{\text{PC}} k_C^{\text{off}} h}{k_C^{\text{on}}} \hat{P}}. \tag{M14}$$

If we rewrite this in a system of units where $\hat{C} = 1$ when $\hat{P} = 0$, we obtain

$$\tilde{C} = \frac{1 + \frac{h k_c^{\text{off}}}{k_C^{\text{on}}}}{1 + \frac{h k_c^{\text{off}}}{k_C^{\text{on}}} + \frac{\hat{R}_{\text{PC}} k_C^{\text{off}} h}{k_C^{\text{on}}} \hat{P}}$$

Now according to [10], $\tilde{C} \approx 1/(1 + 13.3\hat{P})$, which implies that

$$13.3 = \frac{\hat{R}_{\text{PC}} k_C^{\text{off}} h}{k_C^{\text{on}} \left(1 + \frac{h k_c^{\text{off}}}{k_C^{\text{on}}}\right)} = \frac{\hat{R}_{\text{PC}} k_C^{\text{off}} h}{k_C^{\text{on}} + h k_c^{\text{off}}} \rightarrow \hat{R}_{\text{PC}} = 13.3 \left(1 + \frac{k_C^{\text{on}}}{k_C^{\text{off}} h}\right). \tag{M15}$$

4. In [3, Fig. S3i], it is reported that roughly 25% of PAR-6 is bound in wild-type embryos. Assuming that CDC-42 has a similar set of properties, we can assume 25% of the protein is bound. Setting $\hat{K}_C^{\text{on}} = 0.07$ and combining with the inhibition strength (M15) gives about 20% bound CDC-42 at steady state (in dimensional units $k_C^{\text{on}} = 0.1$ μm/s).

5. Let's assume $\hat{C} = 0.25$; then we want to set $\hat{R}_{\text{ACK}}$ to obtain about 25% bound PAR-6 (when there is sufficient PAR-3) as well. Plugging this into the steady state version of (M12g), we obtain

$$\hat{R}_{\text{ACK}}(0.25)(0.75) - (0.0625)(0.25) = 0 \rightarrow \hat{R}_{\text{ACK}} = 0.08 \approx 0.1.$$

6. In embryos depleted of PAR-1 and CHIN-1, the level of PAR-3 at the anterior is roughly 10% of the posterior, and PAR-6 can load onto the membrane everywhere. We therefore set $\hat{A}_0 = 0.06$, since we've already tuned the PAR-3 parameters so that the polarized state has $\hat{A} \approx 0.6$ on the anterior and $\hat{A} \approx 0.06$ on the posterior [5].

7. If $\hat{P} \approx 1$ in the posterior, the parameter $\hat{R}_{\text{PA}}$ can be used to match the distribution of PAR-3 oligomer sizes on the posterior in wild type embryos. As demonstrated in [5], the distribution of oligomer sizes is roughly exponential with exponent $\alpha = \hat{K}_{\text{AP}}^{\text{p}}(\hat{P})\hat{A}_1$. In the absence of PAR-1, $\alpha = 0.42$ on the posterior, giving $(1-\alpha)^2 \approx 30\%$ in monomer form [6]. Setting $\hat{R}_{\text{PA}} = 2$ and substituting $\hat{P} = 1$ in (M12e) gives $\alpha = 0.14$ (85% in monomer form), which is what we use here.

The fitting procedure and values of these seven unknown parameters are summarized Table 2. I have some more stuff about PAR-3 and the other proteins, but not appropriate for this paper.

4 Coupling contractility to biochemistry

We obtain the dimensionless equations which couple biochemistry and contractility via a straightforward combination of (M3) and (M12), advecting all proteins with the myosin flow field [4], and making CDC-42 a promoter of myosin. We also neglect myosin diffusion, since we previously found it to make a negligible contribution to the dynamics, and because bound myosin does not diffuse in the cortex. The resulting equations are

$$\partial_{\hat{t}}\hat{A}_1 + \hat{\sigma}_0\partial_{\hat{x}}\left(\hat{v}\hat{A}_1\right) = \hat{D}_A\partial_{\hat{x}}^2 A_1 + \hat{K}_A^{\rm on}\left(1+\hat{K}_A^{\rm f}\hat{F}_A(\hat{A})\right)\left(1-\int_0^1 \hat{A}(x)\,d\hat{x}\right) - \hat{K}_A^{\rm off}\hat{A}_1 \tag{M16a}$$
$$+ 2\hat{A}_2 - 2\hat{K}_{\rm AP}^{\rm p}{\hat{A}_1}^2 + \sum_{n=3}^{N}\left(\hat{A}_n - \hat{K}_{\rm AP}^{\rm p}\hat{A}_1\hat{A}_{n-1}\right)$$
$$\partial_{\hat{t}}\hat{A}_n + \hat{\sigma}_0\partial_{\hat{x}}\left(\hat{v}\hat{A}_n\right) = \hat{K}_{\rm AP}^{\rm p}\hat{A}_1(\hat{A}_{n-1}-\hat{A}_n) - (\hat{A}_n - \hat{A}_{n+1}) \qquad N > n \geq 2 \tag{M16b}$$
$$\partial_{\hat{t}}\hat{A}_N + \hat{\sigma}_0\partial_{\hat{x}}\left(\hat{v}\hat{A}_N\right) = \hat{K}_{\rm AP}^{\rm p}\hat{A}_1\hat{A}_{N-1} - \hat{A}_N \tag{M16c}$$
$$\partial_{\hat{t}}\hat{C} + \hat{\sigma}_0\partial_{\hat{x}}\left(\hat{v}\hat{C}\right) = \hat{D}_C\partial_{\hat{x}}^2\hat{C} + \hat{K}_C^{\rm on}\left(1-\int_0^1 \hat{C}(\hat{x})\,d\hat{x}\right) - \hat{K}_C^{\rm off}\left(1+\hat{R}_{\rm PC}\hat{P}\right)\hat{C} \tag{M16d}$$
$$\partial_{\hat{t}}\hat{K} + \hat{\sigma}_0\partial_{\hat{x}}\left(\hat{v}\hat{K}\right) = \hat{D}_K\partial_{\hat{x}}^2\hat{K} + \hat{R}_{\rm ACK}\hat{C}\delta_{\hat{A}>\hat{A}_0}\left(1-\int_0^1 \hat{K}(\hat{x})\,d\hat{x}\right) - \hat{K}_K^{\rm off}\hat{K} \tag{M16e}$$
$$\partial_{\hat{t}}\hat{P} + \hat{\sigma}_0\partial_{\hat{x}}\left(\hat{v}\hat{P}\right) = \hat{D}_P\partial_{\hat{x}}^2\hat{P} + \hat{K}_P^{\rm on}\left(1-\int_0^1 \hat{P}(\hat{x})\,d\hat{x}\right) - \hat{K}_P^{\rm off}\left(1+\hat{R}_{\rm KP}\hat{K}\right)\hat{P} \tag{M16f}$$
$$\partial_{\hat{t}}\hat{M} + \hat{\sigma}_0\partial_{\hat{x}}\left(\hat{v}\hat{M}\right) = \hat{K}_M^{\rm on}\left(1+\hat{R}_{\rm CM}\hat{C}\right)\left(1-\int_0^1 \hat{M}(x)\,dx\right) - \hat{K}_M^{\rm off}\hat{M} \tag{M16g}$$
$$\hat{v} = \hat{\ell}^2\partial_{\hat{x}}^2 v + \hat{\ell}\partial_{\hat{x}}\hat{\sigma}_a(\hat{M}) \tag{M16h}$$
$$\hat{R}_{\rm CM} = \frac{r_{\rm CM}C^{(\rm Tot)}}{k_M^{\rm on}},\ \hat{K}_M^{\rm on} = \frac{k_M^{\rm on}}{hk_A^{\rm dp}},\ \hat{K}_M^{\rm off} = \frac{k_M^{\rm off}}{k_A^{\rm dp}},\ \hat{\sigma}_0 = \frac{\sigma_0/\sqrt{\eta\gamma}}{Lk_A^{\rm dp}},\ \hat{\ell} = \frac{\sqrt{\eta/\gamma}}{L}. \tag{M16i}$$

The last equation (M16i) defines the key *new* dimensionless parameters relating to myosin. These differ from (M4) because we can only non-dimensionalize time by one quantity, and we choose here to stick with the depolymerization time $1/k_A^{\rm dp}$. Table 1 gives the dimensional quantities σ_0 and $k_M^{\rm off}$, from which we obtain $\hat{\sigma}_0$ and $\hat{K}_M^{\rm off}$. This leaves two parameters which control the myosin profile: the basal rate $k_M^{\rm on}$, and the amount that CDC-42 promotes myosin, $\hat{R}_{\rm CM}$. In wild-type embryos, we estimate the minimum amount of bound myosin (in the absence of CDC-42) as 0.2. This sets $k_M^{\rm on}$ via $k_M^{\rm on}/(k_M^{\rm on}+k_M^{\rm off}h) \approx 0.2$, giving $k_M^{\rm on} = 0.3$ μm/s. The parameter $\hat{R}_{\rm CM} = 8$ is then chosen to match the initial speed of maintenance phase rescue (flow speed 2 μm/min)

Parameter	Description	Value	Units	Ref	Notes
D_R	Branched actin diffusivity	0.1	μm^2/s		Same as CDC-42
k_R^{off}	Branched actin unbinding rate	0.12	1/s		Same as myosin
$\hat{R}_{\text{CM}}$	C promoting M	8			Fit initial rescue speed
$\hat{C}_R$	Threshold CDC-42 level for branched actin	0.25			Between A and P levels
$\hat{R}_{\text{CR}}$	CDC-42 producing branched actin rate	1			Arbitrary
$\hat{R}_{\text{RR}}$	Autocatalytic branched actin strength	5			Equal strength to nucleation
$\hat{R}_{\text{R}\sigma}$	Branched actin inhibiting myosin rate	10			Fit boundary position

Table 3: Additional parameters for coupled model (M16) with branched actin additions in (M17).

4.1 Incorporating branched actin

In the dimensionless form of (M16), the branched actin equation (3) in the main text is written as

$$\partial_{\hat{t}}\hat{R}+\hat{\sigma}_0\partial_{\hat{x}}\left(\hat{v}\hat{R}\right) = \tag{M17a}$$
$$\hat{D}_R\partial_{\hat{x}}^2\hat{R} + \hat{R}_{\text{CR}}\max\left(\hat{C}-\hat{C}_R,0\right)\left(1+\hat{R}_{\text{RR}}\hat{R}\right)\left(1-\int_0^1 \hat{R}(x)\,dx\right) - \hat{K}_R^{\text{off}}\hat{R},$$

$$D_R = \frac{D_R}{L^2 k_A^{\text{dp}}}, \quad R_{\text{CR}} = \frac{r_{\text{CR}}C^{(\text{Tot})}}{k_A^{\text{dp}}}, \quad R_{\text{RR}} = \frac{r_{\text{RR}}R^{(\text{Tot})}}{r_{\text{CR}}}, \quad \hat{K}_R^{\text{off}} = \frac{k_R^{\text{off}}}{k_A^{\text{dp}}}. \tag{M17b}$$

$$\hat{\sigma}_a = \frac{\hat{M}}{1+\hat{R}_{\text{R}\sigma}\hat{R}}. \tag{M17c}$$

To assign values to the unknown parameters, we assume that branched actin diffuses at the same level as CDC-42, and that the bound lifetime is about 8 s. This gives $D_R = 0.1$ μm/s^2 and $k_R^{\text{off}} = 0.12$. We set the CDC-42 threshold for branched actin nucleation to be between anterior and posterior levels (see Fig. 8 main text), giving $\hat{C}_R = 0.25$. The base level of branched actin production is arbitrary; so we simply set $\hat{R}_{\text{CR}} = 1$, which gives a branched actin level around 0.2 on the anterior. We then assume that branched actin autocatalytic activity makes an equal contribution (relative to CDC-42 nucleation) to the overall branched actin, meaning $\hat{R}_{\text{RR}}\hat{R} = 1$. Since $\hat{R} \approx 0.2$, we get $\hat{R}_{\text{RR}} = 5$. Finally, we set $\hat{R}_{\text{R}\sigma} = 10$, so that the myosin boundary sits roughly at half the domain length. The simulation that results with these parameter values is shown in Fig. 8 of the main text.

4.1.1 Models for peak in myosin

To implement inhibition of myosin by branched actin in simulations, we modify the myosin equation (M16g) so that the unbinding term reads $\hat{K}_M^{\text{off}}\left(1+\hat{R}_{\text{RM}}\hat{R}\right)\hat{M}$. Figure M4(a) shows the resulting

dynamics of rescue when we add this new assumption to our simulation. As before, the myosin and CDC-42 boundary shifts towards the anterior, until CDC-42 exceeds the critical concentration for branched actin. This time, however, branched actin inhibits myosin, which maintains the peak in myosin that initially occurs from flow. The inhibition of myosin, combined with the reduction of tension, actually lead to an imbalance where the boundary post-rescue shifts back towards the posterior, something that we have observed in embryos with extended maintenance phase. The peak in myosin in this case occurs because branched actin is enriched on a smaller domain than myosin, which leaves a medial zone of contractility where myosin is enriched but branched actin is not.

To check the alternative hypothesis of longer myosin lifetime, in Fig. M4(b) we show results of simulations where myosin has a residence time of 25 s instead of 8 s, and there is no longer direct inhibition of myosin by branched actin. Unlike CDC-42, which diffuses in the membrane, in our model there is no diffusivity of myosin, so the longer residence time combines with the existing flows to transport myosin into a peak near 60% embryo length. The peak in this case occurs because of advection of myosin into the zone of contractility.

4.1.2 Models of friction and viscosity

We consider in this section the dimensionless forms of the friction and viscosity relationships in the main text,

$$\gamma(R) = \gamma_0 \left(1 + \hat{R}_{\mathrm{R}\gamma}\hat{R}\right) \qquad \eta(R) = \eta_0 \left(1 + \hat{R}_{\mathrm{R}\eta}\hat{R}\right).$$

Starting from the simulations in Fig. M4(b) (which have increased myosin lifetime to generate a myosin peak), we consider moderate changes in friction/viscosity with branched actin, choosing parameters to roughly double the friction/viscosity on the anterior relative to the posterior (($\hat{R}_{\mathrm{R}\gamma} =$ 10 and $\hat{R}_{\mathrm{R}\eta} = 5$). In Fig. M5, we plot the resulting dynamics of rescue. Both simulations show a maximum in the flow intensity, followed by a gradual decrease in the flow speeds to a steady profile. The simulations with larger viscosity have a flow profile which is smoother (by design), and hence agrees more with experiments, but they tend to smooth the myosin cap so that it becomes almost non-existent. Simulations with increased friction do not show this, but they still retain a small compressive flow in the anterior.

The main distinction between the two models happens when we further increase the dependence of friction/viscosity on branched actin. Suppose, for example that friction is ten times higher (on

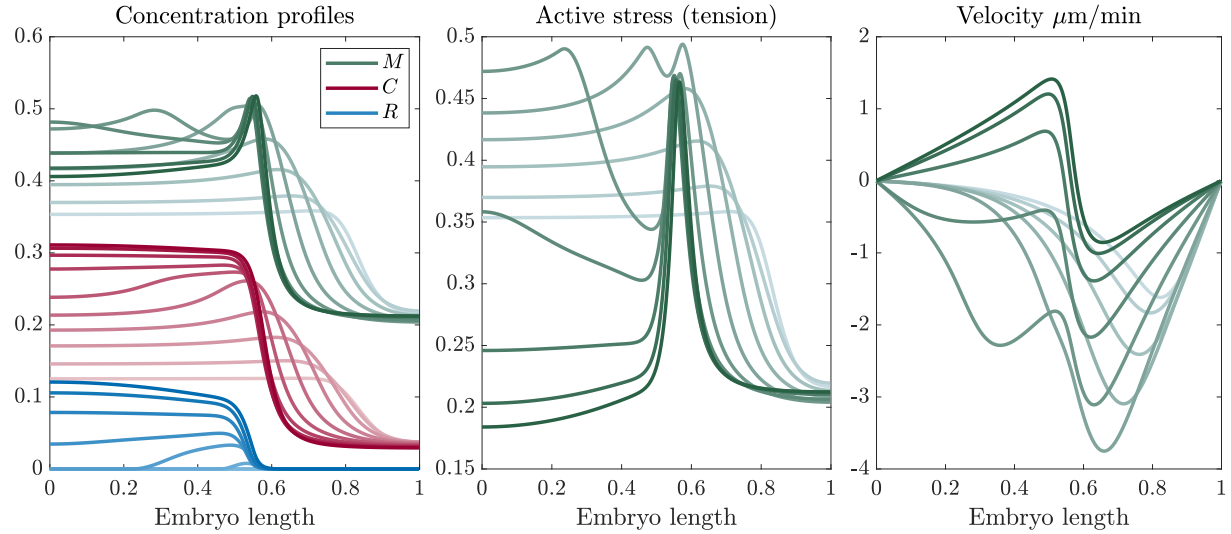

(a) Direct inhibition of myosin by branched actin ($\hat{R}_{\mathrm{RM}} = 2$)

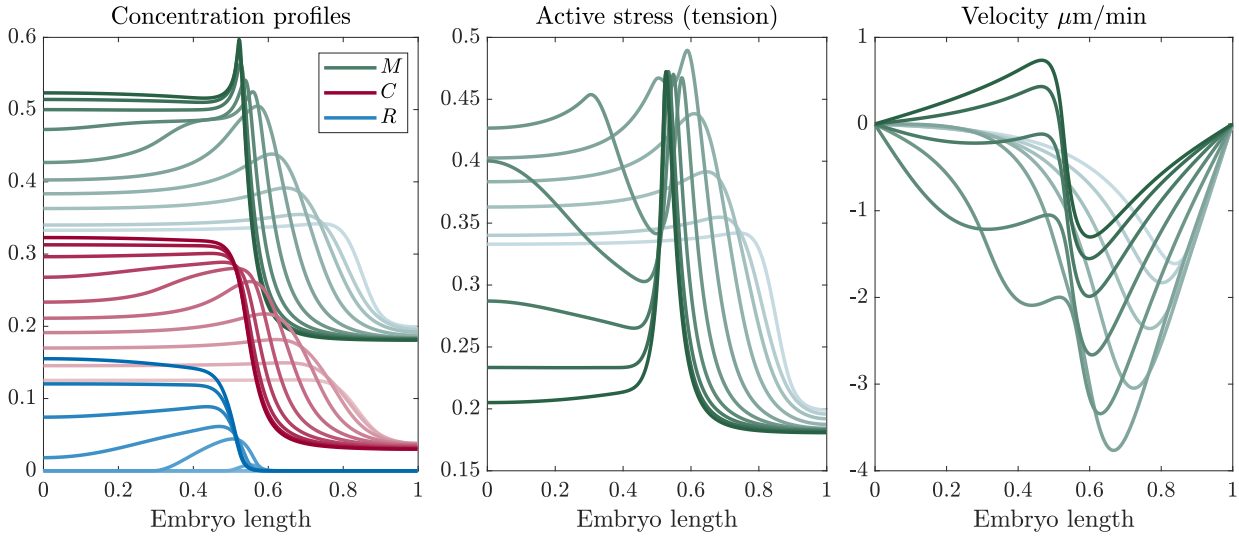

(b) Longer myosin lifetime (25 s)

Figure M4: Two models for how an interior peak of myosin could be maintained. (a) Branched actin directly inhibits myosin in addition to inhibiting stress. (b) The myosin lifetime increases (globally) from 8 s to 25 s. The left panel shows the concentration profile of myosin (M, green), CDC-42 (C, red), and branched actin (R, blue) over time. The middle panel shows the active stress (tension), normalized by σ_0, and the right panel shows the velocity in units of μm/min. Each panel has a series of ten lines which show the profile at $t = 1, 2, \ldots 10$ min, with darker lines showing later times.

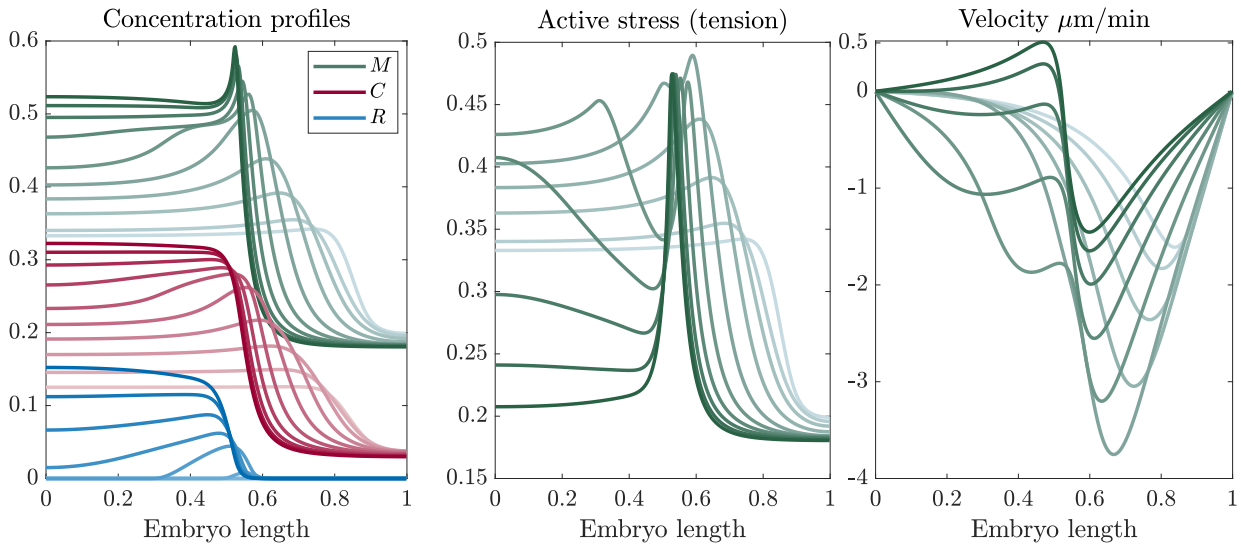

(a) Increased friction ($\hat{R}_{\mathrm{R}\gamma} = 10$)

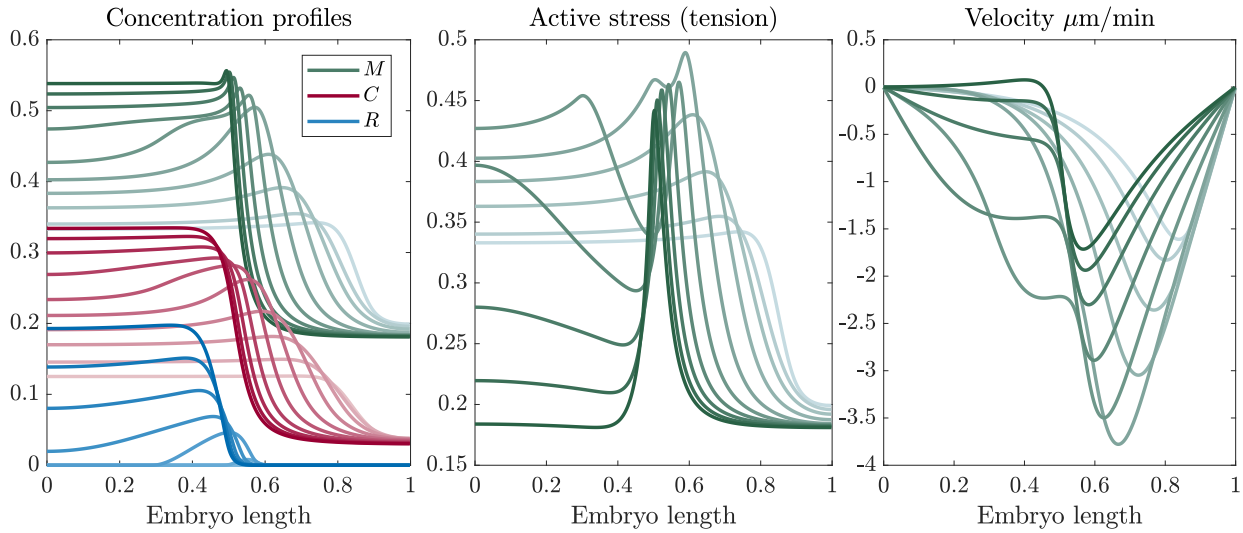

(b) Increased viscosity ($\hat{R}_{\mathrm{R}\eta} = 5$)

Figure M5: Dynamics of rescue when branched actin has *mild* effects on the response to stress. In (a) viscosity is constant and friction increases according to $\gamma(R) = 1 + r_{\mathrm{R}\gamma} R$, while in (b) friction is constant and viscosity increases according to $\eta(R) = 1 + r_{\mathrm{R}\eta} R$. The left panel shows the concentration profile of myosin (M, green), CDC-42 (C, red), and branched actin (R, blue) over time. The middle panel shows the active stress (tension), normalized by σ_0, and the right panel shows the velocity in units of μm/min. Each panel has a series of ten lines which show the profile at $t = 1, 2, \ldots 10$ min, with darker lines showing later times.

the anterior (with branched actin) than in the posterior ($\hat{R}_{\mathrm{R}\gamma} = 100$). Fig. M6(a) shows that this helps the model with increased friction draw closer to the data. We reproduce the sharp drop in velocity when the boundary stalls, and the reduced flows in the anterior preserve the myosin peak for longer (although eventually the peak will disappear because of the weaker velocity). The changes due to friction almost entirely kill the flow in the anterior.

We contrast this with the case where the *viscosity* is five times larger on the anterior (with brached actin) than in the posterior ($\hat{R}_{\mathrm{R}\eta} = 20$), which is shown in Fig. M6(b). Because of the large viscous resistance at the anterior, the rate of strain ($\partial_x v$) has to be constant there. At the anterior cap, the flow is in the negative direction (towards the anterior), and so in high viscosity all that can result is a linear profile moving towards zero at the anterior pole. Put another way, the viscous resistance prevents the velocity profile from rapidly (in space) responding to changes in contractility, and instead of a sharp transition to zero velocity we get a slow transition. The result of this, as shown in Fig. M6 is a boundary which never stops contracting.

4.1.3 Best case parameters

In the last simulation in the main text, we use inhibition of myosin with $\hat{R}_{\mathrm{RM}} = 2$ and a viscosity enhancement factor $\hat{R}_{\mathrm{R}\eta} = 12$.

References

[1] Justin S Bois, Frank Jülicher, and Stephan W Grill. Pattern formation in active fluids. *Biophysical Journal*, 100(3):445a, 2011.

[2] Nathan W Goehring, Philipp Khuc Trong, Justin S Bois, Debanjan Chowdhury, Ernesto M Nicola, Anthony A Hyman, and Stephan W Grill. Polarization of par proteins by advective triggering of a pattern-forming system. *Science*, 334(6059):1137–1141, 2011.

[3] Peter Gross, K Vijay Kumar, Nathan W Goehring, Justin S Bois, Carsten Hoege, Frank Jülicher, and Stephan W Grill. Guiding self-organized pattern formation in cell polarity establishment. *Nature physics*, 15(3):293–300, 2019.

[4] Rukshala Illukkumbura, Nisha Hirani, Joana Borrego-Pinto, Tom Bland, KangBo Ng, Lars Hubatsch, Jessica McQuade, Robert G Endres, and Nathan W Goehring. Design principles

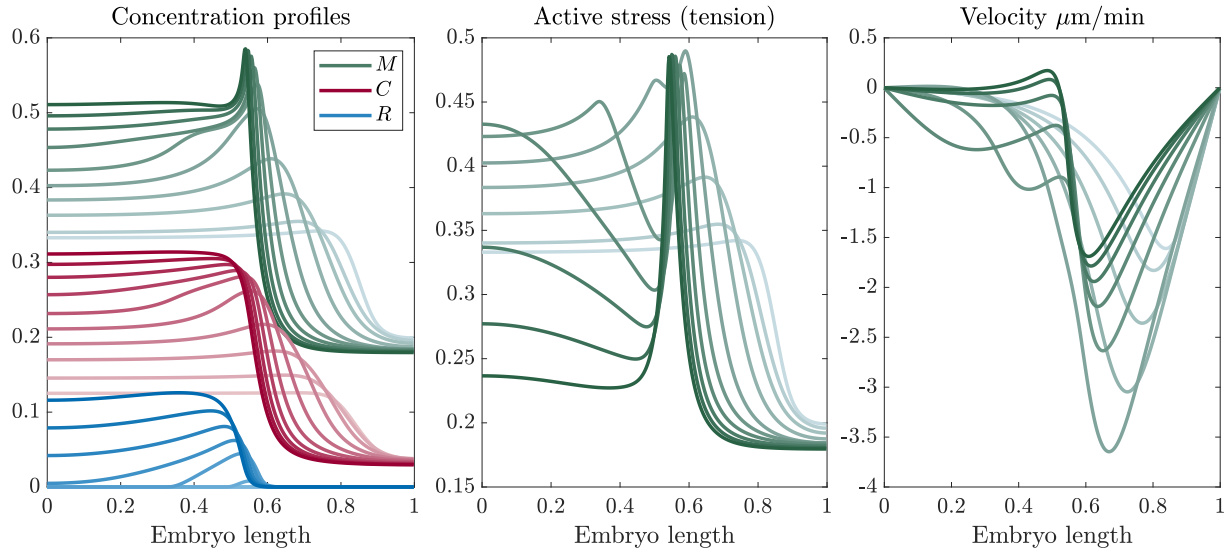

(a) Increased friction ($\hat{R}_{\mathrm{R}\gamma} = 100$)

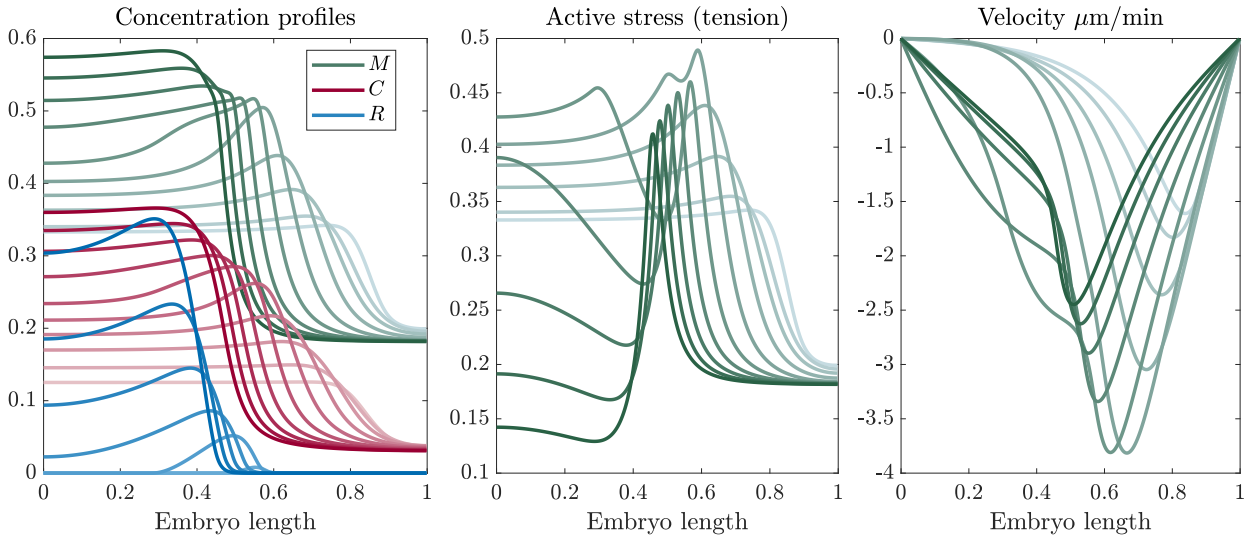

(b) Increased viscosity ($\hat{R}_{\mathrm{R}\eta} = 20$)

Figure M6: Dynamics of rescue when branched actin has *severe* effects on the response to stress. In (a) viscosity is constant and friction increases according to $\gamma(R) = 1 + r_{\mathrm{R}\gamma}R$, while in (b) friction is constant and viscosity increases according to $\eta(R) = 1 + r_{\mathrm{R}\eta}R$ (note the linear velocity gradient where branched actin is enriched). The left panel shows the concentration profile of myosin (M, green), CDC-42 (C, red), and branched actin (R, blue) over time. The middle panel shows the active stress (tension), normalized by σ_0, and the right panel shows the velocity in units of μm/min. Each panel has a series of ten lines which show the profile at $t = 1, 2, \ldots 10$ min, with darker lines showing later times.

for selective polarization of par proteins by cortical flows. *Journal of Cell Biology*, 222(8), 2023.

[5] Charles F Lang, Alexander Anneken, and Edwin Munro. Oligomerization and feedback on membrane recruitment stabilize par-3 asymmetries in c. elegans zygotes. *bioRxiv*, pages 2023–08, 2023.

[6] Charles F Lang and Edwin M Munro. Oligomerization of peripheral membrane proteins provides tunable control of cell surface polarity. *Biophysical Journal*, 121(23):4543–4559, 2022.

[7] Mirjam Mayer, Martin Depken, Justin S Bois, Frank Jülicher, and Stephan W Grill. Anisotropies in cortical tension reveal the physical basis of polarizing cortical flows. *Nature*, 467(7315):617–621, 2010.

[8] François B Robin, William M McFadden, Baixue Yao, and Edwin M Munro. Single-molecule analysis of cell surface dynamics in caenorhabditis elegans embryos. *Nature methods*, 11(6):677–682, 2014.

[9] Arnab Saha, Masatoshi Nishikawa, Martin Behrndt, Carl-Philipp Heisenberg, Frank Jülicher, and Stephan W Grill. Determining physical properties of the cell cortex. *Biophysical journal*, 110(6):1421–1429, 2016.

[10] Anne Sailer, Alexander Anneken, Younan Li, Sam Lee, and Edwin Munro. Dynamic opposition of clustered proteins stabilizes cortical polarity in the c. elegans zygote. *Developmental cell*, 35(1):131–142, 2015.

[11] Yu Chung Tse, Michael Werner, Katrina M Longhini, Jean-Claude Labbe, Bob Goldstein, and Michael Glotzer. Rhoa activation during polarization and cytokinesis of the early caenorhabditis elegans embryo is differentially dependent on nop-1 and cyk-4. *Molecular biology of the cell*, 23(20):4020–4031, 2012.